COBEM 2021 26th International Congress of Mechanical Engineering
ABCM Associação Brasileira de Engenharia e Ciências Mecânicas
November 22-26, 2021, Virtual Congress, Brazil

COB-2021-0809
2-D SIMULATION OF ONE-PHASE FLOW IN NATURALLY FRACTURED RESERVOIRS USING THE EMBEDDED AND THE PROJECTION-BASED EMBEDDED DISCRETE FRACTURE MODELS AND THE MULTI-POINT FLUX APPROXIMATION WITH A DIAMOND STENCIL

André Demski de Oliveira
Twany Mirele Correia
Federal University of Pernambuco - UFPE. Research Institute on Petroleum and Energy-LITPEG. Av. Arquitetura s/n, CEP: 50740-550, Recife, PE, Brazil.
andre.demiski@ufpe.br
twany.correia@ufpe.br

Túlio de Moura Cavalcante
Federal University of Pernambuco - UFPE. Dept. of Civil Engineering & Research Institute on Petroleum and Energy-LITPEG. Av. Arquitetura s/n, CEP: 50740-550, Recife, PE, Brazil.
tulio.cavalcante@ufpe.br

Paulo Roberto Maciel Lyra
Darlan Karlo Elisiário de Carvalho
Federal University of Pernambuco - UFPE. Dept. of Mechanical Engineering & Research on Petroleum and Energy-LITPEG. Av. Arquitetura s/n, CEP: 50740-550, Recife, PE, Brazil.
paulo.lyra@ufpe.br
darlan.ecarvalho@ufpe.br

Abstract. *Naturally Fractured Reservoirs (NFR) are part of the main sources of water and oil worldwide. However, due to the geological complexity and the high contrast of the permeability fields, makes this problem particularly challenging to obtain accurate forecasts and estimates of the production behavior. The study of fluid flow through NFR has advanced steadily over the past years. Despite of that, the numerical modeling and simulation of these reservoirs, involving fractures of different scales is still a great challenge from mathematical and numerical perspective. Aiming to improve computational efficiency, it is interesting to treat the fractures hierarchically, dividing them into similar groups that receive different treatments, accordingly. In this sense, longer fractures, as major conduits or barriers to fluid flow, may be modeled explicitly, context in which an interesting alternative is the use of the Embedded Discrete Fracture Model (EDFM). In this model, each fracture is embedded within the cells of the rock matrix computational mesh with which it intersects, through additional matrix-fracture transmissibilities. It is not necessary to build a mesh fitting the fractures positions. Therefore, EDFM was developed as a technique that may directly incorporates fractures in a conventional structured mesh, bypassing the extra computational cost of using unstructured meshes and remaining compatible with complex fracture geometries. However, previous works show that classic EDFM does not model properly fractures having lower permeability than the rock matrix, on the other hand, a variant of it, called projection-based Embedded Discrete Fracture Model (pEDFM), can effectively deals with these flow barriers. This is achieved through fractures projections on the faces of the rock matrix control volumes, which provides the introduction of additional connections. In this work, we present a strategy to simulate one-phase flow in NFR, in 2-D, using EDFM and pEDFM. In order to solve the pressure equation, we applied a Multi-Point Flux Approximation with a Diamond stencil (MPFA-D), which is a flexible and robust formulation, capable of handling highly heterogeneous and anisotropic media using general polygonal meshes. To validate our scheme, we have solved some representative problems found in literature obtaining promising results.*

Keywords: *Embedded Discrete Fracture Model, Multipoint Flux Approximation, Projection-Based Embedded Discrete Fracture Model.*

1. INTRODUCTION

Naturally Fractured Reservoirs (NFR) are estimated to be most of the remaining exploitable oil fields (Matthäi, 2005), however, due to their geological complexity and the high contrasts permeabilities fields and dimensions, makes this problem particularly challenging to obtain accurate forecasts and estimates of their production behavior. Over the last

years, several studies have been carried out, aiming to develop models that can handle adequately fluid flow in this type of reservoir (Berre et al., 2019). Since it exists, fractures of different scales within NFR, it is interesting to treat them hierarchically, dividing them into similar groups that receive different treatments, accordingly. In this sense, longer fractures, as major conduits or barriers to fluid flow, may be modeled explicitly (Cavalcante et al., 2020). Among the strategies presented in recent years where fractures are modeled explicitly (as additional degrees of freedom), the Embedded Discrete Fracture Modeling (EDFM) (Li and Lee, 2008; Moinfar et al., 2014; Shakiba and Sepehrnoori, 2015) stands out. In this method, each fracture is embedded within the cells of the rock matrix computational mesh with which it intersects, but its discretization is done separately and independently. The fracture and the rock matrix cells in which it is embedded are related through non-neighbor connections (NNCs) and additional matrix-fracture transmissibilities. Therefore, EDFM was developed as a technique that may directly incorporates the influence of fractures in a conventional structured mesh. Thus, bypassing the necessity of the mesh fitting the fractures positions, and the additional computational cost of using unstructured meshes. While remaining compatible with the complex fracture geometries, such as non-straight (or non-planar) fractures or variable aperture fractures (Eigestad, 2004; Berre et al., 2019; Klausen and; Zuo et al., 2019). However, EDFM has showed to be inefficient for the cases where the fracture permeability is much lower than the rock matrix one. Aiming to overcome this limitation, Ţene et al. (2017) proposed a projection-based version of EDFM (pEDFM), which is applicable to both high and low permeability fractures. However, the original pEDFM still had some limitations, especially regarding the method of selecting faces for projection, the calculation of transmissibilities between a fracture and the matrix cells adjacent to that one containing the fracture and the calculation of the projection-based transmissibilities between fractures. These limitations were addressed by the works of Jiang and Younis (2017) and Rao et al. (2020).

The main goal of this work is to model the 2-D one-phase flow in naturally fractured reservoirs using EDFM and pEDFM. In this context, to solve the elliptic pressure equation, we used a finite volume method (FVM) with a non-orthodox Multi-Point Flux Approximation that uses the so-called Diamond stencil (MPFA-D) (Contreras et al., 2016; Gao and Wu, 2011). Our proposed formulation can handle highly heterogeneous and anisotropic domains by using general polygonal meshes, beyond being linearity preserving and capable to achieve second order accuracy on pressure and first order on its gradient. We have combined the robustness and the flexibility of MPFA-D with the low computational cost of EDFM and pEDFM approaches in our simulation tool. We have performed some benchmark tests found in literature in order to validate our scheme and compare EDFM and pEDFM, achieving promising results.

2. MATHEMATICAL MODEL

2.1 Governing Equations

The elliptic pressure equation for one-phase fluid flow can be obtained from the proper manipulation of the general mass balance equation and Darcy's Law:

$$\vec{\nabla} \cdot \vec{v} = Q \quad (with\ \vec{v} = -\boldsymbol{K}\nabla p) \tag{1}$$

where $\vec{\nabla}$, $\vec{v}$, Q, $\boldsymbol{K}$ and p are, respectively, the gradient operator, total velocity, specific total flow rate (source or sink term), absolute permeability tensor, and global pressure. The model considers an isothermal and incompressible fluid flow through porous media, where the effects of gravity and capillarity can be neglected.

3. NUMERICAL FORMULATION

3.1 Multi-Point Flux Approximation with a Diamond stencil (MPFA – D)

The discretization of the pressure equation is made through the MPFA-D (Contreras et al., 2016; Gao and Wu, 2011). Integrating Eq. (1) into a control volume (CV) and applying the Gauss divergence theorem and the mean value theorem, we have:

$$\int_{\Omega} \vec{\nabla} \cdot \vec{v}\, dV = \int_{\partial\Omega} \vec{v} \cdot \vec{n}\, dA = \sum_{i=1}^{n} \vec{v}_i \cdot \vec{N}_i = \bar{Q}V \tag{2}$$

where $\vec{n}$ is the unitary outward normal vector to the control surface $\partial\Omega$, V is the volume (or area, in 2-D) of the CV Ω and A is the area (or length, in 2-D) of the control surface A. $\bar{Q}$ is the mean source term in Ω and n indicates the number of edges in it, considering it is a polygon (part of a polygonal mesh). Aiming to obtain the flux expression for one edge in a 2-D polygonal mesh, we construct the MPFA-D stencil, as shown in Figure 1.

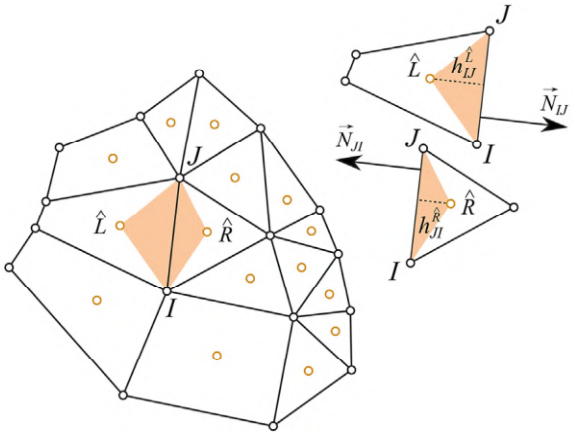

Figure 1. Local diagram of a part of an arbitrary polygonal mesh,
highlighting the "diamond stencil" (Extracted from Cavalcante et al., 2020)

After some algebraic manipulation, the flux continuity equation can be written as (Contreras et al., 2016; Gao and Wu, 2011):

$$\vec{v}_{IJ} \cdot \vec{N}_{IJ} = \tau_{IJ}\left[p_{\hat{R}} - p_{\hat{L}} - \upsilon_{IJ}\left(p_J - p_I\right)\right] \tag{3}$$

where:

$$\tau_{IJ} = -\lambda_{IJ}\frac{K^{(n)}_{IJ_{\hat{L}}}K^{(n)}_{IJ_{\hat{R}}}}{K^{(n)}_{IJ_{\hat{L}}}h^{\hat{R}}_{JI} + K^{(n)}_{IJ_{\hat{R}}}h^{\hat{L}}_{IJ}}\left|\overrightarrow{IJ}\right|;\ \ \upsilon_{IJ} = \frac{\overrightarrow{\hat{L}\hat{R}}\cdot\overrightarrow{IJ}}{\left|\overrightarrow{IJ}\right|^2} - \frac{1}{\left|\overrightarrow{IJ}\right|}\left(\frac{K^{(t)}_{IJ_{\hat{L}}}}{K^{(n)}_{IJ_{\hat{L}}}}h^{\hat{L}}_{IJ} + \frac{K^{(t)}_{IJ_{\hat{R}}}}{K^{(n)}_{IJ_{\hat{R}}}}h^{\hat{R}}_{JI}\right) \tag{4}$$

with:

$$K^{(n)}_{IJ_{\hat{\kappa}}} = \frac{\vec{N}^T\boldsymbol{K}_{\hat{\kappa}}\vec{N}}{\left|\vec{N}\right|^2};\ K^{(t)}_{IJ_{\hat{\kappa}}} = \frac{\vec{N}^T\boldsymbol{K}_{\hat{\kappa}}\overrightarrow{IJ}}{\left|\vec{N}\right|^2};\ \kappa = L, R; \tag{5}$$

where $\vec{N}$ is the area normal vector of the edge IJ. In Eq. (3), $p_{\hat{R}}$ and $p_{\hat{L}}$ are approximations of the pressure value in the right and left control volumes (CVs) of edge IJ. Moreover, the nodal pressures, p_I and p_J are computed using the pressure values at the CVs surrounding nodes I and J, respectively, using a Linear Preserving Weighted Interpolation (Contreras et al., 2016).

3.2 EDFM

The key idea of the EDFM approach is to split the computational domain into a rock matrix domain (Ω_m) and a fracture domain (Ω_f) using two different grids, separately. The coupling is carried out through non-neighbor connections (NNCs) transmissibilities (Moinfar et al., 2014; Shakiba, 2014; Zuo et al., 2019). The pEDFM (Ţene et al., 2017; Jiang and Younis, 2017; Rao et al., 2020) has a similar proposal, with the main difference on the fact that it introduces more alternatives of connections.

3.2.1 Fracture-Matrix coupling connectivity index

Li and Lee (2008) showed that the matrix and fracture grids could be coupled using a transfer function. From a mathematical point of view the transfer function is a source term between the fracture f and the matrix m, which is defined as:

$$q_{f,m} = CI\ \boldsymbol{K}\left(p_f - p_m\right) \tag{6}$$

with CI being the 'connectivity index' between the matrix and the fracture defined as (Hajibeygi et al., 2011):

$$CI^{m-f}_{(x,y),z} = \frac{A_{xy,z}}{\langle d\rangle_{x,y\sim z}}\quad\left(with\ \langle d\rangle_{x,y\sim z} = \frac{1}{A_{x,y}}\int_{A_{x,y}} x\,dA\right) \tag{7}$$

where $(A_{xy,z})$ is the fraction of the area of the fracture element (z) in the matrix cell (x, y) and $\langle d \rangle_{xy,z}$ is the average distance between the fracture element (z) and the matrix cell (x, y).

3.2.2 Fracture-Intersection

If there is an intersection of fractures, their mutual transmissibility can be calculated using the star-delta transformation, as utilized for electrical circuits (Karimi-Fard et al., 2003). The general expression for the transmissibility between fractures o and p, sharing a node connected by n fractures, each one with an aperture w_f^k, and length L^k, is given by:

$$T^{o-p} \simeq \frac{\alpha_o \alpha_p}{\sum_{k=1}^{n} \alpha_k} \quad \left(with \;\; \alpha_k = -2 \frac{K_f^k w_f^k}{L^k} \right) \tag{8}$$

3.3 pEDFM

In pEDFM, the fracture cell *f* is projected at the interfaces Γ_{ij} and Γ_{ik} (in x and y directions, respectively) with the corresponding projection areas (length) denoted by $A_{fm_i}^{px}$ and $A_{fm_i}^{py}$, as shown in Figure 2.

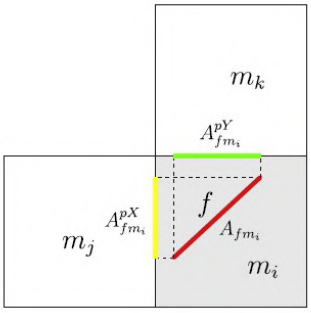

Figure 2. pEDFM schematic representation for a fracture cell (red line) within a matrix cell (Extracted from Jiang and Younis, 2017).

Then, there are *f*-m_j and *f*-m_k connections in addition to *f*-m_i, which already existed in EDFM.

3.3.1 Methods for choosing the faces where the fractures will be projected

The shortest distance method, presented by Jiang and Younis (2017), consists of observing where the center of the fracture cell is located and choosing the face that is closest to it. In this process, we choose a face for the projection in x direction and another face for the projection in y direction. The micro translation method, presented by Rao et al. (2020), is used when the center of the fracture cell is equally distant from two faces, as shown in Figure 2 (in which it occurs in y direction).

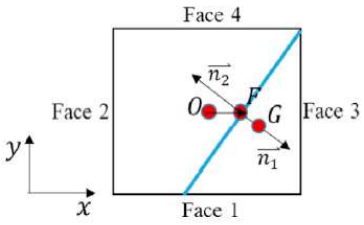

Figure 3. Micro-translation criterion scheme (Extracted from Rao et al., 2020).

Considering a fracture cell *f* contained in a rock matrix cell, we define $\vec{n}_1$ and $\vec{n}_2$ as two opposite normal vectors to *f*, in addition to the vector $\overrightarrow{OF}$ that goes from the center of the matrix cell (O) to the center of the fracture cell (F). Then, we must choose between $\vec{n}_1$ and $\vec{n}_2$ according to the following criterion: $\vec{n} \,.\, \overrightarrow{OF} \geq 0$. In the example shown in Figure 3, $\vec{n}_1$ meets the requirement. The center of fracture cell F is slightly translated to point G along the selected normal vector $\vec{n}_1$. Finally, based on the position of G, we apply "the shortest distance criterion" to select the faces for projection on each

direction. If the distances remain the same, any of the parallel faces can be selected. In the example above, face 3 and face 1 must be selected as the faces for projections.

3.3.2 pEDFM Matrix-Matrix connectivity using MPFA -D

Jiang and Younis (2017) observed that the f-m connections added by pEDFM have effects on the m-m connections. As a consequence, the transmissibilities of the m-m connections should be modified. The area (length) used in the m-m transmissibility expression become the area (length) of the interface between the rock matrix cells minus the area (length) of the union of the fracture projections (of both cells) on this interface, as shown in Figure 4, where the black line represents the union of all fracture cell projections over the Γ_{ij} interface.

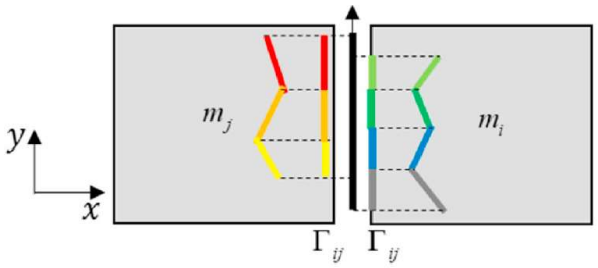

Figure 4. Fracture total projection scheme where the black line is the union of the projected fracture segments on the Γ_{ij} interface (Extracted from Rao et al., 2020).

.

However, our goal is to use MPFA-D instead of TPFA; thus, we needed to adapt the traditional MPFA-D so that it could deal this new requirement. This adaptation was in the expression of the equivalent transmissibility term, expressed initially in Eq. (4), which became:

$$\tau_{IJ} = -\lambda_{IJ} \frac{k_{IJ_{\hat{L}}}^{(n)} k_{IJ_{\hat{R}}}^{(n)}}{k_{IJ_{\hat{L}}}^{(n)} h_{JI}^{\hat{R}} + k_{IJ_{\hat{R}}}^{(n)} h_{IJ}^{\hat{L}}} \left\{ A_{\Gamma_{ij}} - \left[\left(\cup_{r=1}^{n_i} A_{f_r m_i}^{p} \right) \cup \left(\cup_{s=1}^{n_j} A_{f_s m_j}^{p} \right) \right] \right\} \tag{9}$$

where $A_{\Gamma_{ij}}$is the area (length) of the interface Γ_{ij}, n_i and n_j represent the number of fracture segments belonging to m_i and m_j respectively, $A_{f_r m_i}^{p}$represents the projection area (length) of a fracture in m_i and $A_{f_s m_j}^{p}$ represents the projection area (length) of a fracture in m_j.

3.3.3 pEDFM Fracture-Matrix connectivity

Following the work of Rao et al. (2020), we used the following transmissibility expressions to relate a matrix cell (m_i) and a fracture (f):

$$T_{f m_i} = \left(\left(T_{m_i}^{\Omega_2} \right)^{-1} + T_f^{-1} \right)^{-1} \tag{10}$$

$$T_{m_i}^{\Omega_2} = \frac{K_{m_i} A_{f_{m_i}}}{\langle d^{\Omega_2} \rangle}; \; T_f = \frac{K_f A_{f_{m_i}}}{w_f}; \tag{11}$$

$$\langle d^{\Omega_2} \rangle = \frac{\int_{\Omega_2} \vec{n} \cdot \vec{r} \, dV}{V_{\Omega_2}} \approx \frac{\sum_{p \in B} [\vec{n} \cdot \vec{r}(P)]}{|\Upsilon|} \tag{12}$$

where $A_{f_{m_i}}$ is the area (length) of the fracture cell; K_{m_i} is the permeability of m_i; K_f is the fracture permeability; w_f is the fracture aperture; $\vec{n}$ is the unit normal vector obtained as in the micro translation method; $\vec{r}(P)$ is a vector from the center of the fracture cell F to a point P in the matrix cell m_i. Υ is the set of points for which $\vec{n} \cdot \vec{r}(P) < 0$, whose cardinality is $|\Upsilon|$.

3.3.4 pEDFM Fracture-Fracture connectivity

When the fractures in adjacent matrix cells produce overlapping projection, as shown in Figure 5, we have to relate these fractures cells according to the expressions proposed by Rao et al. (2020), with which the transmissibility between $f_r^{m_i}$ within m_i and $f_s^{m_j}$ within m_j, for example, would be as follows:

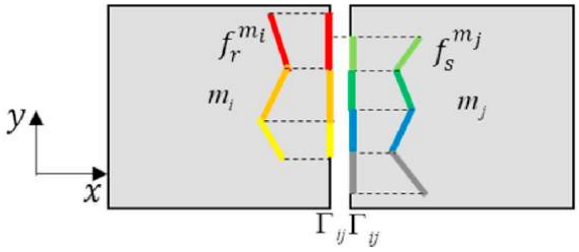

Figure 5. Case with multiple fracture cells in adjacent cells with overlapping projections over the Γ_{ij} interface (Extracted from Rao et al., 2020).

$$T_{f_r^{m_i} f_s^{m_j}} = \left(\left(T_{f_s^{m_j}} \right)^{-1} + \left(T^{\Omega_1 x}_{m_j, f_r^{m_i} f_s^{m_j}} \right)^{-1} + \left(T^{\Omega_1 x}_{m_i, f_r^{m_i} f_s^{m_j}} \right)^{-1} + \left(T_{f_r^{m_i}} \right)^{-1} \right)^{-1} \tag{13}$$

$$T^{\Omega_1 x}_{m_i, f_r^{m_i} f_s^{m_j}} = \frac{K_{m_i} \left(A^p_{f_r^{m_i}} \cap A^p_{f_s^{m_j}} \right)}{\langle d^{\Omega_1} \rangle} \; ; \; T^{\Omega_1 x}_{m_j, f_r^{m_i} f_s^{m_j}} = \frac{K_{m_j} \left(A^p_{f_r^{m_i}} \cap A^p_{f_s^{m_j}} \right)}{\langle d^{\Omega_1} \rangle} \tag{14}$$

$$\langle d^{\Omega_1} \rangle = \frac{\int_{\Omega_1} \vec{n} \cdot \vec{r} \, dV}{V_{\Omega_1}} \approx \frac{\sum_{p \in A} [\vec{n} \cdot \vec{r}(P)]}{|\Lambda|} \tag{15}$$

where $A^p_{f_r^{m_i}} \cap A^p_{f_s^{m_j}}$ is the area (length) intersection of the fracture cell projections $f_r^{m_i}$ and $f_s^{m_j}$, and Λ is the set of points for which $\vec{n} \cdot \vec{r}(P) > 0$.

3.3.5 The extra pEDFM Fracture-Matrix connectivity

The transmissibility expression relating $f_r^{m_i} - m_j$, in its turn, is defined as (Rao et al., 2020):

$$T_{f_r^{m_i} \square_j} = \left(\left(T_{f_r^{m_i}} \right)^{-1} + \left(T^{\Omega_1}_{m_i, f_r^{m_i} \square_j} \right)^{-1} + T^{-1}_{\square_j} \right)^{-1} \tag{16}$$

$$T^{\Omega_1 x}_{m_i, f_r^{m_i} \square_j} = \frac{K_{m_i} \left[A^p_{f_r^{m_i}} - \cup_{s=1}^{\square_j} \left(A^p_{f_r^{m_i}} \cap A^p_{f_s^{m_j}} \right) \right]}{\langle d^{\Omega_1} \rangle} \tag{17}$$

$$T_{\square_j} = \frac{K_{m_j} \left[A^p_{f_r^{m_i}} - \cup_{s=1}^{\square_j} \left(A^p_{f_r^{m_i}} \cap A^p_{f_s^{m_j}} \right) \right]}{d_{f \square_j}} \tag{18}$$

3.4 Discrete Linear System for the Elliptic Pressure Equation

In this work, we consider 2D domains, but, in Ω_f, we deal with a simplified 1D flow, therefore, in this domain, the MPFA-D becomes the classical Two Points Flux Approximation (TPFA) method (Gao and Wu, 2011).

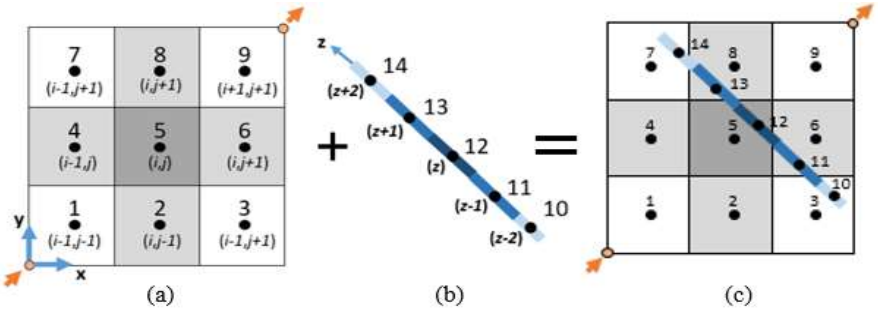

Figure 6. (a) The discrete rock matrix mesh with a central cell 5. (b) The discrete fracture grid with a central cell 12. (c) An example of a discretized domain with one discrete fracture.

If we analyze the flow in cell 5, in the rock matrix grid (figure. 6a), and in cell 12, in the fracture grid Figure. 6b, we have: The F_5^m is understood be the resulting flow in the cell 5 of the rock matrix domain and F_{12}^f the resulting flow in the cell 12 of the fracture domain.

$$\sum F_5^m = F_{2-5}^{m-m} + F_{4-5}^{m-m} + F_{5-6}^{m-m} + F_{5-8}^{m-m} \tag{19}$$

$$\sum F_{12}^f = F_{11-12}^{f-f} + F_{12-13}^{f-f} \tag{20}$$

To complete the formulation of the scheme, and to satisfy the principle of mass conservation for cell 5 and cell 12, we need an NNC, as follows:

$$\sum F_5^{NNC} = F_{5-12}^{m-f} = -F_{12-5}^{f-m} \tag{21}$$

Thus, the total flow in cell 5 can be written as a combination of Eq. (19) and Eq. (21). The same argument is valid for the total flow in cell 12, by combining Eq. (20) and Eq. (21), respecting the flow direction. The discretization of Eq. (19) and Eq. (20) is obtained via the MPFA-D and the TPFA schemes, respectively. However, for Eq. (21) the connectivity index should be used, as presented in Eqs. (6) and (7).

3.5 Solution Strategy

The resultant linear system $\boldsymbol{Tp} = \boldsymbol{F}$ is constructed according to the MPFA-D/TPFA discretization scheme, can be written as:

$$\begin{bmatrix} \boldsymbol{T^{m-m}} & \boldsymbol{T^{m-f}} \\ \boldsymbol{T^{f-m}} & \boldsymbol{T^{f-f}} \end{bmatrix} \begin{bmatrix} \boldsymbol{p^m} \\ \boldsymbol{p^f} \end{bmatrix} = \begin{bmatrix} \boldsymbol{F^m} \\ \boldsymbol{F^f} \end{bmatrix} \tag{22}$$

where, the sub-matrix blocks $\boldsymbol{T^{m-m}}$ and $\boldsymbol{T^{f-f}}$ contain the matrix-matrix and fracture-fracture transmissibility, respectively. The off-diagonal sub-matrices, i.e., $\boldsymbol{T^{m-f}}$ and $\boldsymbol{T^{f-m}}$, contain the transmissibilities between the fractures and matrix. It is worth noting that the linear system above is solved using a sparse iterative linear solver to obtain the pressure field.

4. RESULTS

In this section, we present some results using the MPFA-D formulation coupled with EDFM and pEDFM to simulate some representative 2-D one-phase flow problems in naturally fractured reservoirs. In all the presented problems, the model consists of the classical ¼ of five-spot configuration, considering dimensionless problems. The domain is defined as $\Omega = [0,1] \times [0,1]$ with different arrangements of rock matrix permeabilities and fractures positions. The injection well is placed in the bottom-left corner with pressure set as 1, while the producer well is placed at the top-right corner with the pressure set as zero. No-flow boundary condition is applied at all the external boundaries of the reservoir. The porosities are always set as 0.5 in the rock matrix and 1 in the fractures. The rock matrix properties are referred to by the subscript *m* and the fracture properties are referred to by the subscript *f*. In all examples, we use the *Hybrid-Grid Model* (HyG) (Sandve et al., 2012; Ahmed et al., 2017; Cavalcante et al., 2020;) for the reference case.

4.1 Case 1 - The ¼ five spot one-phase flow with two diagonal channels fractures

In this example, we have two diagonal fractures with aperture $a_f = 5.10^{-2}$ and the rock matrix permeability (K_m) is given by:

$$K_m = \begin{bmatrix} 1 & 0 \\ 0 & 1 \end{bmatrix} \tag{23}$$

The permeability in both fractures K_f is:

$$K_f = 10^5 K_m \tag{24}$$

Figure 7a presents a structured grid with 2500 control volumes used for EDFM and pEDFM models, Figure 7b presents an unstructured grid with 2525 control volumes used for HyG.

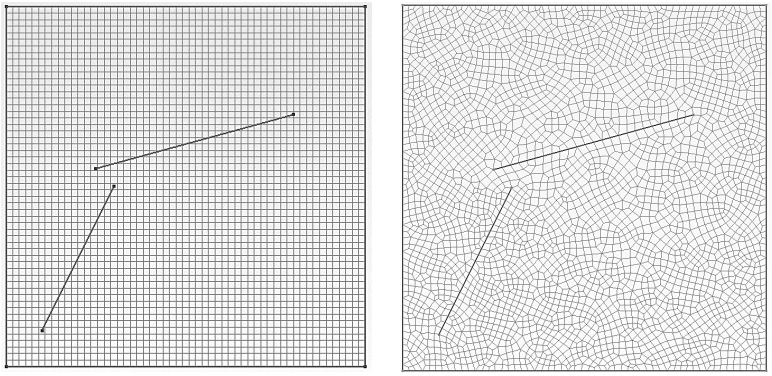

(a) (b)

Figure 7. Meshes used in this test case: (a) for EDFM and pEDFM models; (b) for HyG model.

In order to evaluate the robustness of our formulation, we have compared our results with the results obtained using the MPFA-D/HyG, a method presented by Cavalcante et al. (2020). In Figure 8, we present the pressure fields. As can be seen in Figures 8a and 8b, the results are quite similar qualitative to the reference case (Figure 8c). Figure 8 shows an accentuated pressure gradient, evidencing how the presence of fractures modifies the pressure field of the domain.

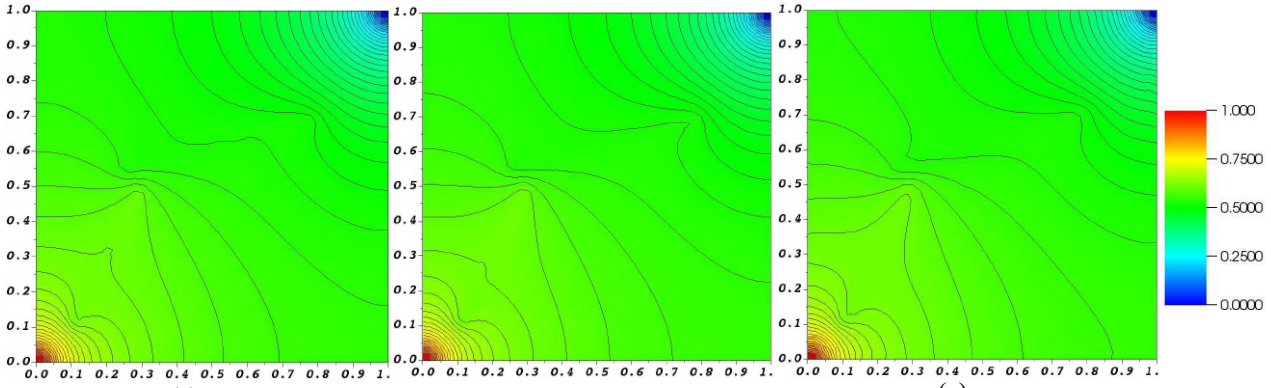

(a) (b) (c)

Figure 8. Pressure fields for case 1: (a) EDFM/MPFA-D; (b) pEDFM/MPFA-D; (c) HyG/MPFA-D.

4.2 Case 2 - The ¼ five spot one-phase flow with one channel and one barrier diagonal fractures

Finally, using the same configurations and geometry shown in Case 1 (Figure 7), modifying only the permeability of the fracture, which was previously of the channel type but in this example, a barrier type with $K_f = 10^{-5}K_m$. The Figure 9 shows the pressure fields for this case, where we can observe through the color maps and the isolines the lack representation in the fracture influence inside the rock matrix by the EDFM modeling (Figure 9a). Otherwise, pEDFM (Figure 9b) and HyG (Figure 9c) modeling can show the fracture presence.

Figure 9a shows a problem already known in the literature for the EDFM, which is not suitable in cases where the fracture permeability value is much lower than the rock matrix permeability value; i.e., cases where the fractures are barriers. To resolve this limitation, pEDFM is shown to be applicable to both, conductive fractures and flow barriers in a very similar way at the reference case.

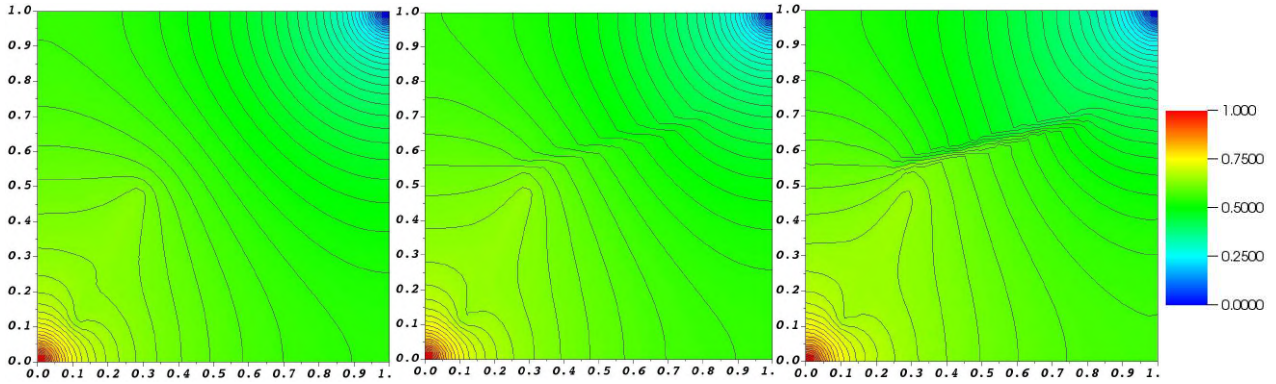

(a) (b) (c)

Figure 9**.** Pressure fields for case 2: (a) EDFM/MPFA-D; (b) pEDFM/MPFA-D; (c) HyG/MPFA-D

5. CONCLUSION

In this work, we have presented a formulation for the numerical simulation of 2-D one-phase fluid flow in naturally fractured petroleum reservoirs. To represent the fracture network, we have used an Embedded Discrete Fracture Model (EDFM) and a projection-based version of EDFM (pEDFM). To solve the elliptic pressure equation in the fractured media, we used a Finite Volume based in a Multipoint Flux Approximation with a Diamond Stencil (MPFA-D). In order to evaluate the accuracy of our MPFA-D/EDFM and MPFA-D/pEDFM formulation we have solved some one-phase flow problems using structured quadrilateral meshes.

For the examples tested in the present article, both EDFM and pEDFM showed results very similar with the reference case. However, the EDFM showed problems in representing their influence in the pressure field in a problem with barrier fractures. Thus, we have used pEDFM which promises to solve this problem through some modifications in EDFM and the results were satisfactory when compared to the reference case, showing the potential of our method to obtain very accurate results at a reasonable computational cost.

6. ACKNOWLEDGEMENTS

The Authors would like to thank the National Council for Scientific and Technological Development (CNPq), the Science Support Foundation of the State of Pernambuco (FACEPE), and the Coordination for the Improvement of Higher Education Personnel (CAPES).

7. REFERENCES

Ahmed, R., Edwards, M. G., Lamine, S., Huisman, B. A. H. and Pal, M., 2017. "CVD-MPFA full pressure support, coupled unstructured discrete fracture–matrix Darcy-flux approximations", *Journal of Computational Physics*, vol. 349, pp. 265–299. https://doi.org/10.1016/j.jcp.2017.07.041.

Berre, I., Doster, F. and Keilegavlen, E., 2019a. "Flow in Fractured Porous Media: A Review of Conceptual Models and Discretization Approaches", *Transport in Porous Media*, vol. 130, no. 1, pp. 215–236. https://doi.org/10.1007/s11242-018-1171-6.

Berre, I., Doster, F. and Keilegavlen, E., 2019b. "Flow in Fractured Porous Media: A Review of Conceptual Models and Discretization Approaches", *Transport in Porous Media*, vol. 130, no. 1, pp. 215–236. https://doi.org/10.1007/s11242-018-1171-6.

Cavalcante, T. de M., Contreras, F. R. L., Lyra, P. R. M. and Carvalho, D. K. E., 2020. "A multipoint flux approximation with diamond stencil finite volume scheme for the two-dimensional simulation of fluid flows in naturally fractured reservoirs using a hybrid-grid method", *International Journal for Numerical Methods in Fluids*, pp. fld.4829. https://doi.org/10.1002/fld.4829.

Contreras, F. R. L., Lyra, P. R. M., Souza, M. R. A. and Carvalho, D. K. E., 2016. "A cell-centered multipoint flux approximation method with a diamond stencil coupled with a higher order finite volume method for the simulation of oil–water displacements in heterogeneous and anisotropic petroleum reservoirs", *Computers & Fluids*, vol. 127, pp. 1–16. https://doi.org/10.1016/j.compfluid.2015.11.013.

Gao, Z. and Wu, J., 2011. "A linearity-preserving cell-centered scheme for the heterogeneous and anisotropic diffusion equations on general meshes", *International Journal for Numerical Methods in Fluids*, vol. 67, no. 12, pp. 2157–2183. https://doi.org/10.1002/fld.2496.

Hajibeygi, H., Karvounis, D. and Jenny, P., 2011. "A hierarchical fracture model for the iterative multiscale finite volume

method", *Journal of Computational Physics*, vol. 230, no. 24, pp. 8729–8743. https://doi.org/10.1016/j.jcp.2011.08.021.

Jiang, J. and Younis, R. M., 2017. "An improved projection-based embedded discrete fracture model (pEDFM) for multiphase flow in fractured reservoirs", *Advances in Water Resources*, vol. 109, pp. 267–289. https://doi.org/10.1016/j.advwatres.2017.09.017.

Karimi-Fard, M., Durlofsky, L. J. and Aziz, K., 2003. "An Efficient Discrete Fracture Model Applicable for General Purpose Reservoir Simulators", In *All Days*, SPE https://doi.org/10.2118/79699-MS.

Klausen, R. A. and Eigestad, G. T., 2004. "Multi Point Flux Approximations and Finite Element Methods; Practical Aspects of Discontinuous Media", In *ECMOR IX - 9th European Conference on the Mathematics of Oil Recovery*, European Association of Geoscientists & Engineers https://doi.org/10.3997/2214-4609-pdb.9.B003.

Li, L. and Lee, S. H., 2008. "Efficient Field-Scale Simulation of Black Oil in a Naturally Fractured Reservoir Through Discrete Fracture Networks and Homogenized Media", *SPE Reservoir Evaluation & Engineering*, vol. 11, no. 04, pp. 750–758. https://doi.org/10.2118/103901-PA.

Matthäi, S. K., 2005. *Modelling multiphase flow in fractured porous rock*, London.

Moinfar, A., Varavei, A., Sepehrnoori, K. and Johns, R. T., 2014. "Development of an Efficient Embedded Discrete Fracture Model for 3D Compositional Reservoir Simulation in Fractured Reservoirs", *SPE Journal*, vol. 19, no. 02, pp. 289–303. https://doi.org/10.2118/154246-PA.

Rao, X., Cheng, L., Cao, R., Jia, P., Liu, H. and Du, X., 2020. "A modified projection-based embedded discrete fracture model (pEDFM) for practical and accurate numerical simulation of fractured reservoir", *Journal of Petroleum Science and Engineering*, vol. 187, pp. 106852. https://doi.org/10.1016/j.petrol.2019.106852.

Shakiba, M., 2014. "Modeling and simulation of fluid flow in naturally and hydraulically fractured reservoirs using embedded discrete fracture model (EDFM)", Retrieved from http://hdl.handle.net/2152/28292.

Shakiba, M. and Sepehrnoori, K., 2015. "Using Embedded Discrete Fracture Model (EDFM) and Microseismic Monitoring Data to Characterize the Complex Hydraulic Fracture Networks", In *Day 3 Wed, September 30, 2015*, SPE https://doi.org/10.2118/175142-MS.

Ţene, M., Bosma, S. B. M., Al Kobaisi, M. S. and Hajibeygi, H., 2017. "Projection-based Embedded Discrete Fracture Model (pEDFM)", *Advances in Water Resources*, vol. 105, pp. 205–216. https://doi.org/10.1016/j.advwatres.2017.05.009.

Zuo, L., Yu, W., Miao, J., Varavei, A. and Sepehrnoori, K., 2019. "Streamline modeling of fluid transport in naturally fractured porous medium", *Petroleum Exploration and Development*, vol. 46, no. 1, pp. 130–137. https://doi.org/10.1016/S1876-3804(19)30012-6.

8. RESPONSIBILITY NOTICE

The authors are the only responsible for the printed material included in this paper.